Impedance Characterization and Modeling of Electrodes for Biomedical Applications

Wendy Franks*, Iwan Schenker, Patrik Schmutz, and Andreas Hierlemann

Abstract—**A low electrode-electrolyte impedance interface is critical in the design of electrodes for biomedical applications. To design low-impedance interfaces a complete understanding of the physical processes contributing to the impedance is required. In this work a model describing these physical processes is validated and extended to quantify the effect of organic coatings and incubation time. Electrochemical impedance spectroscopy has been used to electrically characterize the interface for various electrode materials: platinum, platinum black, and titanium nitride; and varying electrode sizes: 1 cm^2, and 900 μm^2. An equivalent circuit model comprising an interface capacitance, shunted by a charge transfer resistance, in series with the solution resistance has been fitted to the experimental results. Theoretical equations have been used to calculate the interface capacitance impedance and the solution resistance, yielding results that correspond well with the fitted parameter values, thereby confirming the validity of the equations. The effect of incubation time, and two organic cell-adhesion promoting coatings, poly-L-lysine and laminin, on the interface impedance has been quantified using the model. This demonstrates the benefits of using this model in developing a better understanding of the physical processes occurring at the interface in more complex, biomedically relevant situations.**

Index Terms—**Electrochemical impedance spectroscopy, Pt, Pt black, and TiN bioelectrodes.**

I. INTRODUCTION

IMPEDANCE characterization of the electrode-electrolyte interface is of paramount importance in the fields of impedance-based biosensing, neuroprotheses, and *in vitro* communication with electrogenic cells. In impedance-based biosensing, changes in the impedance are correlated to cell spreading and locomotion [1], to bacterial growth [2], to DNA hybridization [3] and to antigen-antibody reactions [4]. Neuroprotheses, and in particular cochlear implants, represent an important application of impedance characterization. The current applied to stimulate hearing via a cochlear implant is determined from the known electrode impedance [5], which is designed to be as low as possible to avoid cell damage [6]. For the extracellular, *in vitro* monitoring of electrogenic cells, where small microelectrodes are required for high-resolution stimulation and recording, the need for a low interface impedance is twofold [7]–[10]. During stimulation a certain current density is necessary to generate activity. A high impedance would result in a large applied electrode voltage leading to undesirable electrochemical reactions that may be harmful to cellular cultures. On the recording side, the extracellular signals are low, on the order of millivolts for cardiomyocytes and microvolts for neurons. The neural signals will be lost in the noisy, ion-based electric fluctuations of the surrounding electrolyte media if the electrode impedance is not low enough. A well-characterized, fully understood interface impedance leads to an optimized electrode-electrolyte interface design.

Equivalent circuit models have long been used to model the interface impedance. In 1899 Warburg first proposed that the interface could be represented by a polarization resistance in series with a polarization capacitor [11]. Experimental findings soon revealed that the polarization capacitance exhibited a frequency dependency leading to the introduction of Fricke's law [12], and the use of a constant phase angle impedance to represent the impedance of the interface capacitance. Randles' work with rapid electrode reaction systems resulted in the well-known Randles model, consisting of an interface capacitance shunted by a reaction impedance, in series with the solution resistance [13]. As the use of platinum electrodes in medical applications became ubiquitous, more research was dedicated to the understanding of the electrode—physiological solution interface. In the case of platinum, the resistive element due to faradaic current was often omitted as measurement equipment was not able to measure at low frequencies where the impedance is finite, and not infinite, as was typically assumed [14]. The work of Schwan and co-workers expanded on previous work to include low frequency considerations [15]. Of particular importance to biomedical applications is Schwan's limit of linearity: the voltage at which the electrode system's impedance becomes nonlinear, which is often exceeded during stimulation [16], [17]. McAdams and colleagues extensively studied the platinum pacing electrode (90% platinum and 10% iridium) in physiological saline, successfully interpreting the frequency-dependent nonlinear interface impedance [18]–[20]. Kovacs has presented an equivalent circuit model based on the Randles model, with an additional Warburg impedance due to the diffusion of faradaic current [7].

In the work presented here, electrochemical impedance spectroscopy (EIS) has been used to characterize the electrode-electrolyte interface for various electrode materials commonly used

*W. Franks is with the Physical Electronics Laboratory, ETH, Zurich 8093, Zurich, Switzerland (e-mail: franks@phys.ethz.ch).

I. Schenker was with the Physical Electronics Laboratory, ETH, Zurich, and is now with the Nonmetallic Inorganic Materials group, ETH Zurich, 8093 Zurich, Switzerland (e-mail: iwan.schenker@mat.ethz.ch).

P. Schmutz is with the Laboratory for Corrision and Materials Integrity, Swiss Federal Institute for Materials Testing and Research (EMPA), 8600 Dübendorf, Switzerland (e-mail: Patrik.Schmutz@empa.ch).

A. Hierlemann is with the Physical Electronics Laboratory, ETH, Zurich 8093, Switzerland (e-mail: hierlema@phys.ethz.ch).

in biomedical applications: platinum, platinum black and titanium nitride. An equivalent circuit model has been used where each parameter represents a macroscopic physical quantity contributing to the interface impedance: The model consists of an interface capacitance, shunted by a charge transfer resistance, in series with the solution resistance. The model parameters have been fitted to the experimental results. To confirm that the parameters do indeed represent the physical quantities, theoretical equations have been used to calculate the parameter values thereby validating the model. With respect to the measurement technique, the effect of the initial interface conditions on the charge transfer resistance is demonstrated. Measurements have been performed for 1 cm^2 bright Pt, Pt black, and TiN, and for 900 μm^2 Pt black. As an extension to models that have been presented in the past [5], [7], [20], this model has been used to quantify the effect of organic cell-adhesion promoting coatings, such as poly-L-lysine (PLL) and laminin, and the effect of incubation time on the interface impedance. This demonstrates the use of the model to develop a complete understanding of the physical processes occurring at the interface in more complex, biomedically relevant situations.

II. METHODS

Both the macroelectrodes and microelectrodes were produced in-house according to the following procedures. For the macroelectrodes a bare p-type Si wafer was electrically isolated with 100 nm SiO$_2$ followed by 500 nm of Si$_3$N$_4$ deposited using plasma enhanced chemical vapor deposition (PECVD). Sputter deposition was used to coat the substrate with 50 nm of TiW, an adhesion promoter, followed by 270 nm of Pt. The wafer was then diced and the chips were cleaned. The chips were then either coated with Pt black or TiN. Pt black was deposited using a 0.3–10 A/cm^2 current density in a solution containing 7 mM hexachloroplatinic acid, 0.3 mM lead acetate and hydrochloric acid to adjust the solution pH to 1.0. Dendritically structured TiN was vapor deposited by the Naturwissenschaftliche und Medizinische Institut at the University of Tübingen, Germany [21]. For the microelectrodes a p-type Si wafer with 100 nm of SiO$_2$ and 500 nm of Si$_3$N$_4$ was used as the substrate. As above, 50 nm TiW and 270 nm Pt were sputter deposited, and the microelectrodes with leads and bond pads were structured in a lift-off process. The wafer was passivated with 500 nm Si$_3$N$_4$. A reactive-ion etch (RIE) was used to open the electrodes, thereby defining their size and shape. The wafer was then diced, and the chips cleaned. The bond wires of the packaged chips were encapsulated in polydimethylsiloxane (PDMS) for electrical isolation.

Bright Pt macroelectrodes were coated with two different cell-adhesion promoting coatings, laminin, and poly-L-lysine, in the following manner. The samples were cleaned with an air plasma treatment (2 min. at $\sim$3.0(10)$^{-2}$ mbar). It is known from x-ray photon spectroscopy (XPS) measurements that, immediately following plasma cleaning, the surface contains no carbon, indicating that the surface is free of organic residues. Additionally, plasma cleaning has the effect of activating the surface and is believed to lead to better quality protein layers with respect to coverage and adhesion. Within 45 min of

plasma cleaning the protein coatings were applied. Samples were incubated (37 °C, 5% CO$_2$) overnight in laminin (20 mg/ml phosphate buffered saline, PBS). For PLL the samples were incubated for 30 min in a 0.05% solution. After incubation the samples were rinsed three times with PBS.

To investigate the effect of time on the interface impedance, bright Pt samples were incubated in medium containing 10% horse serum. Impedance measurements were performed after 7, 14, and 35 days using medium with serum as the electrolyte.

Measurements were performed using a commercially available Autolab PGSTAT30 potentiostat system with Frequency Response Analysis software (version 4.9, Eco Chemie B.V., Netherlands). In this three-electrode system, a standard calomel electrode (SCE) is the reference electrode, the counter electrode is large-area Pt, and the electrolyte is physiological saline, 0.9% NaCl. In addition to the time dependency measurements, neuron medium with 10% horse serum was used as the electrolyte in one set of measurements. The perturbation potential was 10 mV and the scan range was 10^{-3} to 10^5 Hz, unless otherwise noted. Measurements were typically performed with respect to the open-circuit potential (OCP), the potential naturally occurring between the working and reference electrodes. The OCP is a function of the chemical composition of the interface, and can significantly affect the impedance results. Accordingly, special attention was paid to the preparation of the samples to ensure that the interface was as defined as possible. It is known that organic residues on the substrate surface can contribute to a faradaic current, which decreases the charge transfer resistance and polarizes the electrode. An *in situ* cleaning process was, therefore, used where the Pt and Pt black electrodes (without coatings) were treated by voltammetric cycling from -1.0 to 1.0 V for typically 6 cycles, at which point the measurement stabilized. Cyclic voltammetry potentially results in the formation and reduction of Pt oxide and Pt dioxide layers, as indicated by the Pt-H$_2$O Pourbaix diagram [22]. Since the OCP is a function of the interface composition, the OCP can be altered through the cycling process. Additionally, the OCP can be used as a quality control to ensure that the initial conditions are the same from measurement to measurement. The average OCP values for Pt, Pt black, and TiN were $0.318 \pm 0.037, 0.299 \pm 0.061$, and 0.046 ± 0.034 V, respectively. The relatively large range of OCP values for TiN can be attributed to the fact that the samples were not treated with cyclic voltammetry for fear of damaging the dendritic structure.

Measurements were first performed with relatively large area samples (1 cm^2) to establish the measurement technique and equivalent circuit model under stable experimental conditions. Difficulties with respect to stability were encountered during the measurement of the microelectrodes as the current approached the system measurement limit of 10 nA at low frequencies. As a result, the frequency range for the microelectrode measurements was reduced to 10^{-2} to 10^5 Hz.

III. EQUIVALENT CIRCUIT MODEL

The equivalent circuit model presented in this work comprises a constant phase angle impedance Z_{CPA}, that represents the interface capacitance impedance, shunted by a charge
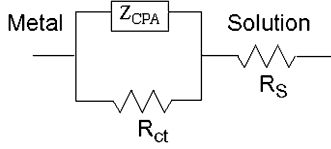
Fig. 1. Equivalent circuit model of electrode-electrolyte interface.

transfer resistance R_{ct}, together in series with the solution resistance R_S, see Fig. 1, [23]. This model is an adaptation from the theoretical models typically used to represent the electrode-electrolyte impedance [7], [19], [24]. The Warburg impedance due to diffusion of the chemical reactants in solution is not included in this model. For the materials and frequency range employed here, it was experimentally determined that the Warburg impedance does not significantly contribute to the overall impedance.

A. Interface Capacitance

The constant phase angle impedance is a measure of the non-faradaic impedance arising from the interface capacitance, or polarization, and is given by the empirical relation [20]

$$Z_{CPA}(\omega) = \frac{1}{(j\omega Q)^n} \quad (1)$$

where Q is a measure of the magnitude of Z_{CPA}, n is a constant $(0 \leq n \leq 1)$ representing inhomogeneities in the surface and $\omega = 2\pi f$. In a Nyquist plot the angle between the data and the abscissa axes gives n according to $n = (2\theta)/\pi$. When $n = 1$, Z_{CPA} represents a purely capacitive impedance element corresponding to the interface capacitance.

A theoretical derivation of the interface capacitance is given by the Gouy-Chapman-Stern model (GCS) [25]. The interface capacitance is taken to be the series combination of the double-layer capacitance, termed the Helmholz capacitance C_H, and the diffuse layer capacitance, the Gouy-Chapman capacitance C_G, and is given by the following formula:

$$\frac{1}{C_I} = \frac{1}{C_H} + \frac{1}{C_G} = \frac{d_{OHP}}{\varepsilon_0\varepsilon_r} + \frac{L_D}{\varepsilon_0\varepsilon_r \cosh\left(\frac{z\phi_0}{2U_t}\right)} \quad (2)$$

where d_{OHP} is the thickness of the double-layer, ε_0 is the permittivity of free space, ε_r is the permittivity of the double layer, z is the charge on the ion in solution, ϕ_0 is the applied electrode potential, and U_t is the thermal voltage. The Debye length, L_D, is given by

$$L_D = \sqrt{\frac{\varepsilon_0\varepsilon_r U_t}{2n^0 z^2 q}} \quad (3)$$

where n^0 is the bulk number concentration of ions in solution and q is the elementary charge. See Table I for the values of the constants and variables used here.

B. Equilibrium Exchange Current Density and R_{ct}

At equilibrium, equal, and opposite reduction and oxidation currents flow across the electrode-electrolyte interface. The magnitude of these currents is termed the equilibrium exchange current density J_0 and is given by

$$J_0 = Fk_c c_A e^{(-\beta F \Delta\phi_0)/(RT)} \quad (4)$$

TABLE I
SUMMARY OF THE VALUES USED FOR VARIABLES AND CONSTANTS USED TO CALCULATE THE THEORETICAL VALUE OF C_I USING (2). IN THE "NOTE" COLUMN ALL ASSUMPTIONS ARE GIVEN

Parameter	Value	Note
d_{OHP}	5 Å	Physiological saline at 25 °C [7]
ε_0	$8.85(10)^{12}$ F/m	
ε_r	78	Dilute aqueous solution at 25 °C [25]
z	4	O_2 reduction reaction [29]
U_t	0.0259 V	
n^0	$9.3(10)^{25}$ ions/m³	Physiological saline at 25 °C
q	$1.602(10)^{-19}$ C	

for the reduction reaction where F is Faraday's constant, k_c is reduction reaction rate constant, c_A is the concentration of electron-acceptor ions A in solution plane of the interface, β is the symmetry factor, $\Delta\phi_0$ is the equilibrium potential, R is the gas constant and T is the temperature [26]. The equilibrium current is a measure of the electrode's ability to participate in exchange current reactions, and, hence, is of particular relevance to this work. For an ideally polarizable electrode J_0 equals zero and for an ideally unpolarizable electrode J_0 tends to infinity; in reality, J_0 lies somewhere between these two extremes. It is tempting to use literature values of J_0 to compare various electrode materials, however, since J_0 is a function of ion concentration and temperature, literature values must be carefully considered.

The equilibrium exchange current and R_{ct} can be experimentally determined through the application of the low-field approximation to the Butler-Volmer equation $(\eta < 0.005/z)$, which yields

$$J = \frac{J_0 F \eta}{RT} \quad (5)$$

where J is the measured current density, η is the applied overpotential, z is the number of electrons involved in the redox reaction, and $RT/F = 26$ mV at 298 K. Under the low-field approximation, the Butler-Volmer equation reduces to Ohm's law. A plot of the current versus overpotential yields a straight line and the charge transfer resistance is given by the slope as $R_{ct} = RT/(J_0 z F)$. Cyclic voltammetry was used to determine J_0 under the following conditions: 5 mV perturbation signal with respect to the OCP, 0.5 mV/s scan rate, 0.15 mV step potential, averaged over 10 scans. For the case of Pt the charge transfer arises from the electrolysis of H_2O and reduction of O_2 according to $2H_2O \leftrightarrow O_2 + 4H^+ + 4e^-$ where the equilibrium potential is

$$0.987 - 0.059 \times pH \quad (6)$$

with respect to the SCE [27]. For the calculation of J_0, z was, therefore, assumed to be 4. It should be noted that the presence of contaminants at the interface will also contribute to the faradaic current.

C. Solution Resistance

The resistance measured between the working electrode and the reference electrode is termed the solution resistance. It can
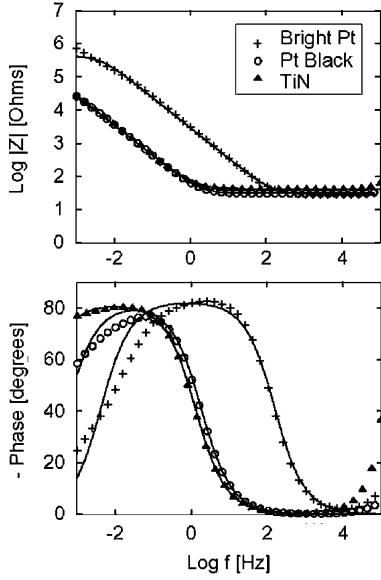
Fig. 2. Impedance modulus and phase as a function of frequency for 1 cm² Pt, Pt black, and TiN electrode materials [28]. Modeled results are indicated by the smooth lines.

TABLE II
SUMMARY OF THE AVERAGED, FITTED PARAMETER RESULTS, WITH CORRESPONDING STANDARD DEVIATIONS, FOR THE FOLLOWING MATERIALS AND MEASUREMENT AREAS: BRIGHT Pt 1 cm², Pt BLACK 1 cm², TiN 1 cm², Pt BLACK MICROELECTRODE 900 μm², PLL-COATED BRIGHT Pt 1 cm², LAMININ-COATED BRIGHT Pt 1 cm², BRIGHT Pt WITH NEURON MEDIUM AS THE ELECTROLYTE, 1 cm²

	Q $[\text{s}\Omega^{-1/n}]$	n	R_s $[\Omega]$	R_{ct} $[\Omega]$
Pt	$2.72(10)^{-5}$	0.92	28.0	$4.48(10)^5$
Std. dev.	$0.26(10)^{-5}$	0.01	2.81	$0.88(10)^5$
Pt black	$2.08(10)^{-3}$	0.91	30.7	$5.11(10)^4$
Std. dev.	$0.11(10)^{-3}$	0.03	7.85	$2.88(10)^4$
TiN	$2.03(10)^{-3}$	0.91	42.3	$3.00(10)^5$
Std. dev.	$5.77(10)^{-5}$	0.00	3.70	$3.20(10)^5$
μelectrode Pt black	$0.86(10)^{-9}$	0.86	$7.38(10)^3$	$2.70(10)^9$
Std. dev.	$0.52(10)^{-9}$	0.02	$1.74(10)^3$	$1.31(10)^9$
PLL	$8.57(10)^{-6}$	0.91	37.0	$1.24(10)^6$
Std. dev.	$0.51(10)^{-6}$	0.01	2.41	$0.69(10)^6$
Laminin	$5.00(10)^{-6}$	0.89	28.3	$2.46(10)^5$
Std. dev.	$2.88(10)^{-6}$	0.01	5.64	$0.68(10)^5$
Neuron Medium	$1.46(10)^{-5}$	0.91	40.4	$4.26(10)^5$
Std. dev.	$0.18(10)^{-5}$	0.01	2.30	$0.57(10)^5$

be determined from the spreading resistance, the resistance encountered by current spreading out into solution, under the assumption that the counter electrode is infinitely large and the working electrode is surrounded by electrolyte. The spreading resistance is given by

$$R_s = \frac{\rho \ln 4}{\pi l} \qquad (7)$$

for square electrodes (ρ is the solution resistivity, 72 Ωcm for physiological saline [7], l the electrode side length), and

$$R_s = \frac{\rho}{4r} \qquad (8)$$

for round electrodes (r is the radius) [7]. It is worth noting that unlike R_{ct} and C_I, which scale with the total electrode area, the solution resistance is dependent upon the geometric area only (where geometric area refers to the planar two-dimensional area, and not the larger total area which increases with roughness).

IV. RESULTS

EIS measurements and model results for 1 cm² Pt, Pt black, and TiN are given in Fig. 2, [28]. Table II gives a summary of the averaged, fitted parameter values with corresponding standard deviations. For Q, n, and R_s the standard deviation is 10%, or less, in almost all cases. In the case of R_{ct} the standard deviation is as high as 110%. This large standard deviation can be attributed to the high sensitivity of R_{ct} to the electrode-electrolyte interface conditions. Furthermore, R_{ct} is extrapolated from the low frequency data which leads to increased uncertainty. The sharply decreasing phase angles at high frequencies is an artifact of the measurement system.

A. Verification of Model Parameters

To confirm the validity of the model, the model parameters have been calculated based on the theoretical principles presented above. A comparison between the fitted and theoretical parameters has been performed for the simplest case of bright
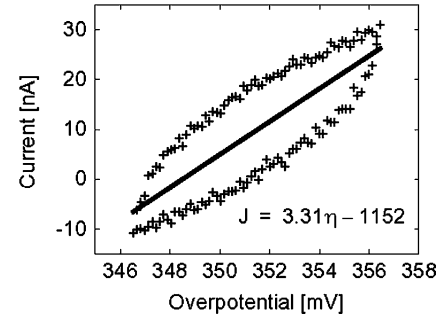

Fig. 3. Equilibrium exchange current density measurement: current versus applied electrode overpotential measurement results for 1 cm² bright platinum. A ± 5 mV overpotential with respect to an OCP of 351.5 mV was applied.

Pt. Using (2) and the variable values given in Table I, the theoretical interface capacitance was found to be 0.545 F/m². The impedance of the interface capacitance was calculated using $Z_{C_I} = (j\omega C_I)^{-1}$, and at an angular frequency of 1 s^{-1}, $|Z_{C_I}|$ is $1.83(10)^4$ Ω (for 1 cm²). Similarly, using the values of Q and n (given in Table II) for 1 cm² bright Pt, and (1), $|Z_{CPA}|$ was found to be 1.59×10^4 Ω. For R_{ct}, cyclic voltammetry was used to generate a current versus overpotential plot, see Fig. 3. From the slope of the plot, R_{ct} was found to be 300 kΩ; the fitted value was found to be 450 kΩ. From (5), the exchange current density was calculated to be $8.5(10)^{-8}$ A/cm². Finally the solution resistance was determined to be 32.0 Ω using (8). The fitted parameter value is 28.0 Ω.

B. Effect of OCP on Model Results

Throughout the course of this work it has been observed that the model parameter R_{ct} is highly dependent on the initial electrode-electrolyte interface conditions. To demonstrate this dependance, the OCP was set to various values, either by cyclic voltammetry or by an applied potential. The EIS phase results (the modulus results show no variation) and the fitted values for R_{ct} are given in Fig. 4.
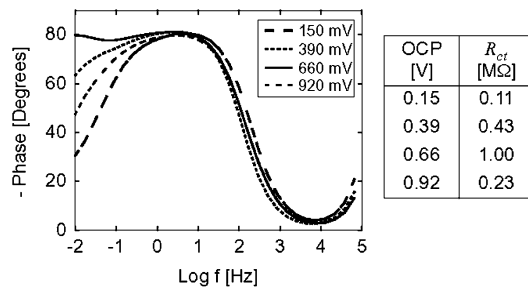
Fig. 4. Effect of OCP on measurements results. Measurements were performed using 1 cm² bright platinum samples. The table shows the fitted values for R_{ct}.
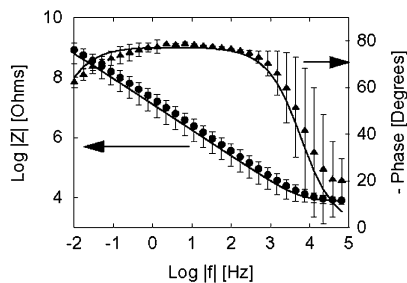

Fig. 5. Impedance modulus and phase experimental results for Pt black microelectrodes (geometrical area 900 μm^2). The modeled results are indicated by the solid lines [28].

C. Microelectrode Results

The impedance modulus, phase, and standard deviations for the Pt black microelectrodes (geometric area 900 μm^2) are presented in Fig. 5; fitted parameter values are given in Table II. A variation in the total electrode area within the sample population arising from the platinization procedure results in a large measurement standard deviation apparent in the phase measurements at high frequencies. The theoretical value for the interface capacitance, 0.545 F/m² [from (2)] and the relation $\text{area}_{\omega=1 \text{ s}^{-1}} = |Z_{\text{CPA}}|/|Z_{C_I}|$, which simplifies to $\text{area} = Q_n/C_I$, were used to determine the total area of each of the 6 microelectrodes measured. The areas ranged from $8.36(10)^3$ to $45.5(10)^3$ μm^2, with a standard deviation of $17.2(10)^3 \mu m^2$. Development of a more uniform platinization process is currently under investigation.

D. Effect of Coatings and Neuron Medium as Electrolyte

Fig. 6 shows the impedance modulus and phase results for the two cell—adhesion promoting coatings, laminin (n = 7) and PLL (n = 5), and for the measurements performed with neuron medium (n = 4) as the electrolyte (see Table II for fitted parameter values). The charge transfer resistance of PLL and laminin is 1.24 and 0.25 MΩ, respectively, a difference which quantifies the relative reactivity of the materials at the given conditions. For the PLL and laminin coatings the value for Q was found to be 8.6 and 5.0 $\mu s/\Omega^{-1/n}$, respectively. In the case of the neuron medium as the electrolyte, the parameter value for R_{ct} is similar to that of bright Pt. The value of Q was found to be 14.6 $\mu s/\Omega^{-1/n}$ which is smaller than that of bright Pt. The solution resistance of the neuron medium was found to be 40.4 Ω, which yields a value of 90.3 Ωcm [from (8)] for the neuron medium resistivity.
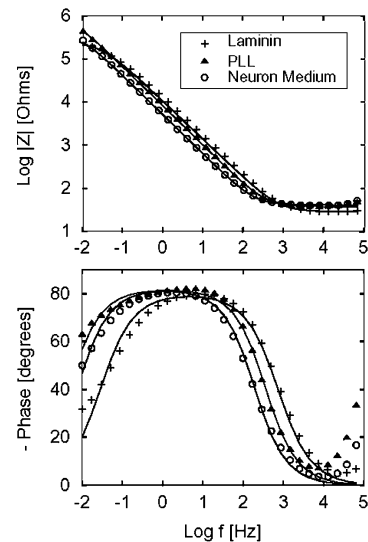

Fig. 6. Impedance modulus and phase for the laminin and PLL protein coatings, and the neuron medium as electrolyte. The modeled results are indicated by the solid lines.
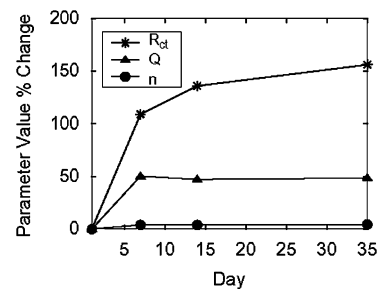

Fig. 7. Relative change in modeled parameter value as a function of time for 1 cm² bright Pt incubated in medium containing 10% horse serum for up to 35 days.

E. Effect of Time

The percent change in model parameter results for impedance recordings performed at days 1, 7, 14, and 35 in incubation are given in Fig. 7. In all cases, the parameter value increases from day 1 to day 7, and then levels off. This demonstrates the effective encapsulation of the electrodes, as is discussed in the following section.

V. DISCUSSION

An equivalent circuit model has been used to describe and analyze the EIS experimental results. A good match between the curves generated using the equivalent circuit model and the measurement results indicates that the appropriate model has been selected. For the simplest case of bright Pt, equations describing the macroscopic physical processes occurring at the electrode-electrolyte interface yield parameter values for C_I and R_S that are in good agreement with the experimentally derived parameters. The difference between $|Z_{C_I}|$ and $|Z_{\text{CPA}}|$ represents a 15% deviation from the experimental value, which is evidence that the GCS model describes well the interface capacitance. The difference between the fitted and calculated theoretical value could be a result of impurities at the interface that are not accounted for in the GCS model. A 14% deviation from

the measured value of the solution resistance indicates that (7) can be used to calculate R_S.

Cyclic voltammetry was used to measure R_{ct} for the bright Pt-0.9% NaCl system. There is a 50% difference between the fitted R_{ct} value and that determined from cyclic voltammetry. The source of this difference is difficult to quantify, however, is most likely a result of sensitivities, in both the EIS and the cyclic voltammetry measurements, to the interface conditions. It is worthwhile to mention that the R_{ct} value reported here is four orders of magnitude greater than the values reported in literature, $\sim 30 \ \Omega \text{cm}^2$ [10], [29]. The literature values are erroneously based on the assumption that the faradaic current flowing across the interface is due to a hydrogen redox reaction. For a neutral pH, the equilibrium potential of the hydrogen reaction is -0.654 V, significantly negative of the OCP value of 0.318 ± 0.037 V. Given the positive OCP value, the theoretical reaction would be the oxidation of hydrogen gas according to: $\text{H}_2 \leftrightarrow 2\text{H}^+ + 2\text{e}^-$, although the limited amount of hydrogen gas available in solution precludes this reaction from occurring. It is known from literature that, given the experimental conditions used in this work, it is the O_2 redox reaction that is mainly responsible for the faradaic current (although contamination at the interface will also contribute to charge transfer) [27]. Experiment results presented here support this assumption. When the OCP is set to value higher or lower than the equilibrium value of approximately 0.6 V [from (6) using a pH of 7.0], the R_{ct} is lower than if the OCP were equal to the equilibrium value. The higher or lower potential shifts the reaction from equilibrium conditions, more faradaic charge transfer occurs, and R_{ct} is reduced. For example, for an OCP of 0.66 V the change transfer resistance is 1.0 MΩ (Fig. 4). For an OCP of 0.39 and 0.92 V the charge transfer resistance reduces to 0.43 MΩ and 0.23 kΩ, respectively. Since R_{ct} depends on J_0, it is interesting to compare the J_0 value measured here with those reported in literature. The value reported by Kovacs for the oxygen reaction is $4.5(10)^{-6}$ A/cm^2, which was experimentally determined using a platinum electrode and aerated frog Ringer's solution (115 mM NaCl, 2.0 mM KCl, 1.8 mM CaCl$_2$) [7], [30]. Aeration of the electrolyte will increase the amount of O_2 available for reaction, thereby increasing the equilibrium exchange current, which explains the deviation from the value reported here. The value reported by McAdams [19] for a platinum pacing electrode in physiological saline is $6.41(10)^{-8}$ A/cm^2, which is similar to our measured value of $8.5(10)^{-8}$ A/cm^2, albeit a direct comparison is invalid due to the 10% iridium content in the pacing electrode.

It has been the goal of this study to use the EIS results and model parameter values to develop an enhanced understanding of the effect of the physical processes on the interface impedance, with the expressed purpose of improving the interface design. For example, the impedance modulus of Pt black and TiN is two orders of magnitude smaller than for bright Pt, clearly demonstrating the effect of increased total surface area. This finding is expected and is well documented in previous studies [10], [29], [31]. A more interesting use of the results can be found in the effects of PLL and laminin on the interface impedance. Qualitatively, there is little difference between the impedance modulus of PLL and laminin, however, the phase results show that the phase decreases more rapidly for laminin

that PLL, indicating a lower R_{ct} for laminin. Quantitatively, this difference manifests itself in the fitted parameter results, where R_{ct} is 1.24 MΩ for PLL versus 0.25 MΩ for laminin. Although laminin is a thicker coating ~ 140 nm compared to PLL ~ 10 nm, it appears to facilitate charge transfer rather than to impede reactions. The effect of the coating thicknesses is apparent in the modeled parameter Q, which is approximately $1/3$ of Q for bright Pt. Since is representative of the interface capacitance, which is inversely proportional to the "dielectric" thickness (in this case the coating), it follows that the coatings would reduce Q. Such effects are important when considering an optimized interface design for the stimulation and recording of electrical activity from electrogenic cells, or when designing biosensors based on changes in the interface capacitance.

Additionally, the model has been used the quantify the effect of incubation time on the interface impedance. The relative change in the model parameter results over time show a sharp increase from day 1 to 7, followed by a plateau. Indeed, the impedance results themselves (not shown here) do not change significantly from day 7 to 35. This indicates that the electrodes have been encapsulated, most likely by proteins contained in the medium. For example, the value of n increases from 0.91 at day 1 to 0.95 at day 35, indicating that the interface has become more capacitive. Similarly, R_{ct} increases from 217 kΩ at day 1 to 556 kΩ at day 35, again demonstrating that the interface has become more capacitive, or less conducive to charge transfer. The same is true of Q, which increases from an initial value of 6.5 $\mu\text{s}/\Omega^{-1/n}$ to 9.7 $\mu\text{s}/\Omega^{-1/n}$ by day 35. These results are relevant to researchers who are performing electrophysiological measurements over extended periods of time. The changing electrode impedance of electrodes covered by cell cultures would additionally provide useful insights and shall be investigated in the future.

The ease in analyzing surface conditions using EIS and its widespread applicability gives merit to a short discussion on how this technique may be extended to other electrode-electrolyte systems and smaller electrode sizes. In order to use this technique with different systems, such as iridium oxide, gold, stainless steel and other biomedical metals with electrolytes of varying concentrations and compositions, the appropriate equivalent circuit, which is highly dependent on the equilibrium exchange current density, must be selected. For nonpolarizable electrodes, corresponding to a high equilibrium exchange current, the charge transfer resistance becomes low and a Warburg element, representing the effect of diffusion on the current-carrying ions, may be necessary to accurately model the interface conditions (the reader is referred to general references on EIS [25], [26], [32]). Due to the sensitivity of J_0 to the interface conditions, as demonstrated in this work, the equilibrium exchange current varies significantly with electrode and electrolyte and, hence, care must be taken when using values from literature. It is, therefore, recommended that J_0 be experimentally determined. Although values for J_0 are reported in literature, for example Kovacs provides a table with various values [7], it is unlikely that the experimental conditions are exactly the same. Pourbaix diagrams may be used to determine the reactions giving rise to J_0, and will provide a value for z that is required to determine R_{ct} using (5). Many cases of EIS applied

to different electrode-electrolyte systems can be found in literature, for example: Bates, *et al.*, have analyzed a system of roughened Pt and aqueous H_2SO_4 [33], Valoen, *et al.*, have developed an impedance model for metal hydride electrodes in KOH [34], and Chou and colleagues have used EIS to investigate the effect of a self-assembled monolayer on a Au electrode inside a rat heart [35]. As a final extension to the model, it should be noted that while this theory may be applied to infinitely small electrodes, the experimental measurement becomes increasingly unstable with shrinking electrode dimensions because the current flowing across the interface becomes too small to be measured. Very small electrodes, $\sim 100 \ \mu m^2$, must be measured at higher frequencies requiring special equipment.

VI. CONCLUSION

A measurement technique with a corresponding equivalent circuit model has been established for the quantification of the electrode-electrolyte interface impedance using electrochemical impedance spectroscopy. Equations describing the macroscopic physical processes occurring at the interface are presented, and, for the case of bright Pt, yield results that are in good agreement with the fitted parameter values. The effect of various characteristics, such as total area, protein coating, and time on the EIS and fitted parameter results has been used to elucidate the processes occurring at the interface, thereby demonstrating the usefulness of the model in the impedance analysis of more complex, biomedically relevant situations.

ACKNOWLEDGMENT

REFERENCES

[1] J. Wegener, C. R. Keese, and I. Giaever, "Electric cell-substrate impedance sensing (ECIS) as a noninvasive means to monitor the kinetics of cell spreading to artificial surfaces," *Exp. Cell Res.*, vol. 259, pp. 158–166, 2000.

[2] L. Yang, C. Ruan, and Y. Li, "Detection of viable salmonella typhimurium by impedance measurement of electrode capacitance and medium resistance," *Biosensors Bioelectron.*, vol. 19, no. 5, pp. 495–502, 2003.

[3] C. A. Marquette, I. Lawrence, C. Polychronakos, and M. F. Lawrence, "Impedance based DNA chip for direct T_m measurement," *Talanta*, vol. 56, pp. 763–768, 2002.

[4] V. M. Mirsky, M. Riepl, and O. S. Wolfbeis, "Capacitive monitoring of protein immobilization and antigen-antibody reactions on monomolecular alkylthiol films on gold electrodes," *Biosensors Bioelectron.*, vol. 12, pp. 977–989, 1997.

[5] C. Q. Huang, R. K. Shepherd, P. M. Center, P. M. Seligman, and B. Tabor, "Electrical stimulation of the auditory nerve: Direct current measurement *in vivo*," *IEEE Trans. Biomed. Eng.*, vol. 46, no. 4, pp. 461–469, Apr. 1999.

[6] M. Tykocinski, Y. Duan, B. Tabor, and R. S. Cowan, "Chronic electrical stimulation of the auditory nerve using high surface area (HiQ) platinum electrodes," *Hearing Res.*, vol. 159, pp. 53–68, 2001.

[7] G. T. A. Kovacs, "Introduction to the theory, design, and modeling of thin-film microelectrodes for neural interfaces," in *Enabling Technologies for Cultured Neural Networks*, D. A. Stenger and T. M. McKenna, Eds. London, U.K.: Academic, 1994, pp. 121–165.

[8] G. W. Gross, B. K. Rhoades, D. L. Reust, and F. U. Schwalm, "Stimulation of monolayer networks in culture through thin-film indium-tin oxide recording electrodes," *J. Neurosci. Methods*, vol. 50, pp. 131–43, 1993.

[9] P. Thiebaud, C. Beuret, M. Koudelka-Hep, M. Bove, S. Martinoia, M. Grattarola, H. Jahnsen, R. Rebaudo, M. Balestrino, J. Zimmer, and Y. Dupont, "An array of Pt-tip microelectrodes for extracellular monitoring of activity of brain slices," *Biosensors Bioelectron.*, vol. 14, pp. 61–65, 1999.

[10] M. O. Heuschkel, "Fabrication of multielectrode array devices for electrophysiological monitoring of *in vitro* cell/tissue cultures," in *Series in Microsystems*, P. A. Besse, M. Gijs, R. S. Popovic, and Ph. Renaud, Eds. Konstanz, Germany: Hartung-Gorre Verlag, 2001, vol. 13.

[11] E. Warburg, "Ueber das Verhalten sogenannter unpolarisbarer Elektroden gegen Wechselstrom," *Annalen der Physik und Chemie*, vol. 67, pp. 493–499, 1899.

[12] H. Fricke, "The theory of electrolytic polarization," *Philosophical Mag.*, vol. 7, pp. 310–318, 1932.

[13] J. E. B. Randles, "Kinetics of rapid electrode reactions," *Discussions Faraday Soc.*, vol. 1, pp. 11–19, 1947.

[14] D. Jaron, H. P. Schwan, and D. B. Geselowitz, "A mathematical model for the polarization of cardiac pacemaker electrodes," *Med. Biol. Eng.*, vol. 6, p. 579, 1968.

[15] B. Onaral and H. P. Schwan, "Linear and nonlinear properties of platinum electrode polarization. I. Frequency dependence at very low frequencies," *Med. Biol. Eng. Comput.*, vol. 20, pp. 299–306, 1982.

[16] H. P. Schwan, "Electrode polarization impedance and measurements in biological materials," *Ann. New York Acad. Sci.*, vol. 148, pp. 191–209, 1968.

[17] ——, "Linear and nonlinear electrode polarization and biological materials," *Ann. Biomed. Eng.*, vol. 20, pp. 269–88, 1992.

[18] E. McAdams, "Effect of surface topography on the electrode-electrolyte interface impedance," *Surface Topogr.*, vol. 2, pp. 107–122, 1989.

[19] E. T. McAdams and J. Jossinet, "Physical interpretation of Schwan's limit voltage of linearity," *Med. Biol. Eng. Comp.*, vol. 32, pp. 126–30, 1994.

[20] E. T. McAdams, A. Lackermeier, J. A. McLaughlin, D. Macken, and J. Jossinet, "The linear and nonlinear electrical properties of the electrode-electrolyte interface," *Biosensors Bioelectron.*, vol. 10, pp. 67–74, 1995.

[21] M. Janders, U. Egert, M. Stelzle, and W. Nisch, "Novel thin film titanium nitride micro-electrodes with excellent charge transfer capability for cell stimulation and sensing applications," in *Proc. IEEE Eng. Med. Biol. Soc.*, Amsterdam, The Netherlands, 1997.

[22] M. Pourbaix, *Atlas of Electrochemical Equilibria in Aqueous Solutions*, 2nd ed. Brussels, Belgium: National Association of Corrosion Engineers, 1974.

[23] W. Franks, F. Heer, I. McKay, S. Taschini, R. Sunier, C. Hagleitner, A. Hierlemann, and H. Baltes, "CMOS monolithic microelectrode array for stimulation and recording of natural neural networks," presented at the Transducers'03, Boston, MA, 2003.

[24] D. C. Grahame, "Mathematical theory of the faradaic admittance," *J. Electrochem. Soc.*, vol. 99, pp. 370C–385C, 1952.

[25] A. J. Bard and L. R. Faulkner, *Electrochemical Methods*. New York: Wiley, 2001.

[26] J. O. M. Bockris and A. K. N. Reddy, *Modern Electrochemistry*. New York: Plenum, 1970, vol. 2.

[27] E. Yeager, "Electrocatalysts for O2 reduction," *Electrochimica Acta*, vol. 29, pp. 1527–1537, 1984.

[28] F. Heer, W. Franks, A. Blau, S. Taschini, C. Ziegler, A. Hierlemann, and H. Baltes, "CMOS microelectrode array for monitoring of electrogenic cells," *Biosensors Bioelectron.*, vol. 20, pp. 358–366, 2004.

[29] D. A. Borkholder, "Cell based biosensors using microelectrodes," Ph.D. Thesis, Stanford Univ., Stanford, CA, 1998.

[30] P. W. Davies, "The oxygen cathode," in *Physical Techniques in Biological Research*, W. L. Nastuk, Ed. London, U.K.: Academic, 1962, vol. IV, pp. 137–179.

[31] J. D. Weiland, D. J. Anderson, and M. S. Humayun, "In vitro electrical properties for iridium oxide versus titanium nitride stimulating electrode," *IEEE Trans. Biomed. Eng.*, vol. 49, no. 12, pp. 1574–1579, Dec. 2002.

[32] J. R. Macdonald, *Impedance Spectroscopy*. New York: Wiley, 1987.

[33] J. Bates and Y. Chu, "Electrode-electrolyte interface impedance: Experiments and model," *Annals of Biomed. Eng.*, vol. 20, pp. 349–363, 1992.

[34] L. O. Valeon, S. Sunde, and R. Tunold, "An impedance model for electrode processes in metal hydride electrode," *J. Alloys Compounds*, vol. 253–254, pp. 656–659, May 20, 1997.

[35] H. A. Chou, D. H. Zavitz, and M. Ovadia, "*In vivo* CH_3 $(CH_2)_{11}$ SAu SAM electrodes in the beating heart: *in situ* analytical studies relevant to pacemakers and interstitial biosensors," *Biosens. Bioelectron.*, vol. 18, pp. 11–21, 2003.

Wendy Franks received the B.Sc. degree in chemical engineering in 1998 and the M.Sc. degree in electrical engineering in 2000, both at the University of Waterloo, Waterloo, ON, Canada. She received the Ph.D. degree from the Swiss Federal Institute of Technology, Zurich (ETHZ) in the field of bioelectronics.

Patrik Schmutz received an undergraduate degree in solid-state physics in 1991 from the University of Fribourg, Switzerland, and a Ph.D. degree in science in 1996 from the Swiss Federal Institute of Technology in Lausanne (EPFL).

He is currently Head of Corrosion Research at the EMPA (National Laboratory for Material Science and Technology) and is a Lecturer at the Swiss Federal Institute of Technology in Zurich (ETHZ), Switzerland. His main research topic is investigation of localized physico-(electro)chemical processes on reactive metallic surfaces.

Iwan Schenker received the Diploma in physics from the Swiss Federal Institute of Technology (ETHZ), Zurich, Switzerland, in 2003. He is currently working towards the Ph.D. degree in the Nonmetallic Inorganic Materials Group, Department of Materials, ETHZ, Zurich, Switzerland.

Andreas Hierlemann received the Diploma in chemistry in 1992 and the Ph.D. degree in physical chemistry in 1996 from the University of Tübingen, Tübingen, Germany.

Having been a Postdoc at Texas A&M University, College Station, TX (1997), and Sandia National Laboratories, Albuquerque, NM (1998), he is currently Professor at the Physical Electronics Laboratory at ETH Zurich in Switzerland. The focus of his research activities is on CMOS-based microsensors and interfacing CMOS electronics with electrogenic cells.